Journal of Molecular Graphics and Modelling 50 (2014) 78–89

Contents lists available at ScienceDirect

Journal of Molecular Graphics and Modelling

journal homepage: www.elsevier.com/locate/JMGM

# Study on the disulfide bond and disulfide loop of native and mutated SOD1 protein

S.P. Keerthana, P. Kolandaivel*

*Department of Physics, Bharathiar University, Coimbatore 641 046, India*

ARTICLE INFO

*Article history:*
Accepted 7 March 2014
Available online 6 April 2014

*Keywords:*
Disulfide loop
Disulfide bond
Cu–Zn superoxide dismutase 1
A4V mutation
Molecular Dynamics

ABSTRACT

The superoxide anions in the human body are reduced into hydrogen peroxide and molecular oxygen by the metallo enzyme Cu–Zn superoxide dismutase 1. The disulfide bond in SOD1 is essential to maintain the structural stability of protein and its proper folding. A computational study on the disulfide bond with the addition of residues was made using three different level of theories viz., B3LYP/6-31G (d,p), M052X/6-31G (d,p) and MP2/6-31G (d,p). The nature of disulfide bond was found to be unaffected with the additional residues being attached to the termini of cysteine residues. This result was found to be in agreement with the experimental values. The results of Molecular Dynamics simulation illustrate the crinkled appearance caused in the disulfide loop of A4V mutation. The conformational change in the disulfide loop was found to have significant effect on the loss of dimerization, metal binding affinity and overall protein stability. It is also noted that the disulfide loop with more number of residues is found to have no effect on the disulfide bond characteristics, but the disulfide loop with less number of residues is found to have remarkable effect for mutation in any position of the wild type protein.



## 1. Introduction

The human copper–zinc superoxide dismutase 1 [Cu–Zn SOD1] is a homodimeric protein which catalyses the dismutation of superoxide radical into hydrogen peroxide and oxygen [1]. Each sub unit of the homodimer is found to possess one $Cu^{2+}$ ion and $Zn^{2+}$ ion, two free cysteines Cys 111 and Cys 6 in reduced form and two oxidized form of cysteines Cys 57 and Cys 146 involved in disulfide linkage [2–5]. The stability of the intramolecular disulfide bond is important to maintain the stability of quaternary and tertiary structure of SOD1 [6]. The disulfide bond (S—S) between the residues Cys 57–Cys 146 is found to be interesting, since it connects the metal coordination loop IV to the central β-sandwich [7,8]. The formation and breaking of S—S bonds have been occurred in many biological macro-molecules such as proteins, enzymes and antibiotics, where the disulfide bridge or disulfide linkage is found to play a vital role in maintaining the stability of particular conformation and to increase the biological activity [9]. The missense mutations at more than 150 positions in Cu–Zn superoxide dismutase 1 (SOD1) have been found to cause A-myotrophic lateral sclerosis (ALS), an invariably fatal neuro degenerative disease characterized by loss of motor neurons in the brain [10]. Familial ALS suggests that SOD1 is more susceptible to intramolecular disulfide bond and accelerate protein turnover [11]. Mutation in the disulfide loop is responsible for neurotoxicity of SOD1 [12]. The function of disulfide loop involves the metal binding process at the active-site. The S—S bond is important to maintain the three dimensional structure of protein and its stability [13]. The disulfide loop of monomer A in native Cu–Zn SOD1 protein [PDB CODE: 1HL5] [14–16] having residues from 49 to 62 and 146 is shown in Fig. 1 as ball and stick coloured in magenta.

We studied the role of additional residues to the disulfide bond by adding residues to each cysteine terminals. The characteristics of disulfide bond of cysteine residues are studied computationally both in gas and solvent phases. The computational results were compared with the experimental results obtained for the same protein structure. The disulfide bond along with the additional residues is subjected to Molecular Dynamics [MD] simulation. The disulfide loop of the SOD1 protein in native and A4V mutated states were also subjected to MD simulation. The MD simulations were carried out for the period of 30 ns both in solvent and vacuum environments. Analyses of the trajectories give an overview of the conformational changes of disulfide loop in A4V mutant. Among 150 mutations in SOD1, A4V mutation is found to be very dangerous, because, once the mutation is caused, the life span of the patient reduced to 1½ years [17]. The variations in the structural parameters during simulation are analyzed both in solvent and vacuum phases. The conformers with disulfide bond and additional residues were taken from the simulated structures and those conformers were

* Corresponding author. Tel.: +91 422 2428441; fax: +91 422 2425706.
*E-mail addresses:* ponkvel@hotmail.com, ponkvel@buc.edu.in (P. Kolandaivel).

http://dx.doi.org/10.1016/j.jmgm.2014.03.002
1093-3263/

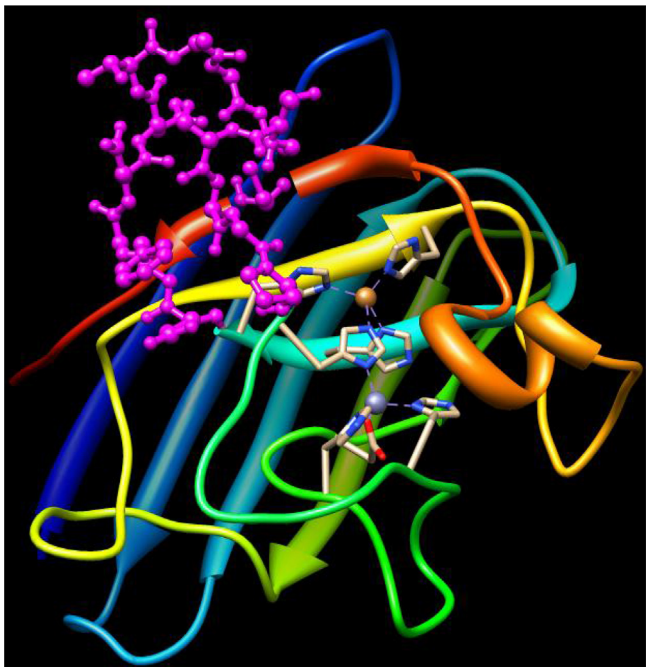

**Fig. 1.** The monomer A of native Cu–Zn SOD1 protein which has the pdb code of 1HL5. The disulfide loop is represented in terms of ball and stick coloured in magenta.

examined by AIM (Atoms in Molecules) analysis technique. The topological parameters for all the structures were calculated. All these calculations explained the nature of disulfide bond in native structure along with the influence of additional residues. Natural bond analysis has been performed to study the charge transfer mechanism of sulfur atom due to the addition of residues. The reactivity indices calculation has been used to identify the electrophilic and nucleophilic nature of sulfur atoms. So the aim of the present investigation is to study the disulfide bond in SOD1 protein and the conformational change of disulfide loop due to A4V mutation in the protein. These two studies are very important to understand the role of S—S bond in the function of SOD1 protein.

## 2. Computational details

All the theoretical calculations were performed in gas and solvent phases using Gaussian 09 program package [18]. The Becke's three parameter functional along with Lee–Yang–Parr's [LYP] gradient corrected correlational functional, i.e., B3LYP [19,20] and hybrid meta generalized gradient approximation (GGA) method M052X [21,22] have been employed with the 6-31G (d,p) basis set to optimize the dipeptide, tripeptide, tetrapeptide and hexapeptide structures. Møller Plesset Perturbation theory [23] has been employed with the 6-31G (d,p) basis set to optimize the above structures. The same level of theory has been used for the frequency calculations and no negative frequencies were observed. Hence all the structures are minima on the potential energy surface. The geometrical parameters and characteristics of S—S bond were analyzed from the optimized geometries of the studied structures.

The stability of the disulfide bond was analyzed using natural bond analysis technique [24]. The topological analysis was performed to calculate the charge density and its second derivative of Laplacian electron density for the S—S bond using Bader's Atoms in Molecules [AIM] theory [25]. The condensed Fukui functions were calculated using the procedure proposed by Yang and Mortier based on Mulliken Population Analysis [MPA] on the three possible forward, backward and central finite approximations to the derivatives.

$$f(r) = \left(\frac{\delta\mu}{\delta v(r)}\right)_N = \left(\frac{\partial\rho(r)}{\partial N}\right)_{v(r)}$$

We obtain

$$f_k^-(r) = q_k(N) - q_k(N-1)$$

governing electrophilic attack

$$f_k^+(r) = q_k(N+1) - q_k(N)$$

governing nucleophilic attack

$$f_k^0(r) = \frac{1}{2}q_k(N+1) - q_k(N-1)$$

governing radical attack

Where $f_k^-$ and $f_k^+$ describe the ability of an atom to accommodate an extra electron or a loss of an electron and $f_k^0$ is considered as indicator for radical reactivity. The different conformations with disulfide bond in gas and solvent phases at B3LYP/6-31G (d,p), M052X/6-31G (d,p) and MP2/6-31G (d,p) level of theories was studied by performing the Potential Energy Scan [PES] analysis. The PES for various peptide structures was calculated varying the dihedral angle by 30° between the atoms C3–S1–S2–C4.

The MD simulations were carried out using GROMACS [26] suite of programs [version 4.5.5]. The OPLSAA [27,28] force field was used to describe the intramolecular disulfide bond along with additional residues and the residues in the disulfide loop of Human SOD1 protein [PDB structure 1HL5] [14–16]. The disulfide loop residues were placed in cubic box of edge length 1 nm, which was subsequently filled with SPC [29,30] water molecules for simulation in solvent environment and no water molecules will be filled in vacuum environment. A cut-off 1.4 nm was used for Lennard–Jones interactions. The coulomb and van der Waals interactions between atoms within 1.0 nm were evaluated at every time step. The Particle Mesh Ewald method [31–34] was employed to treat coulomb interactions. For energy and pressure, the long-range dispersion correction was employed. Using the Berendson barostat and thermostat the constant pressure and temperature is maintained by weak coupling of the system to an external bath at 1 bar and 300 K respectively. The coupling time of 0.1 ps was used to couple the system with the temperature bath. The isothermal compressibility was at $4.5 \times 10^{-5}$ bar and the pressure coupling time was 0.5 ps. The constraints for all the bonds were imposed using the LINCS algorithm. The MD integrator was used with an integration time step of 2 fs. The conformational change for the disulfide loop in A4V mutated state where the alanine at codon 4 is replaced by valine [35] is shown in Fig. 2 for 0, 3, and 30 ns and compared with the native disulfide loop for the same period of time.

## 3. Results and discussion

### 3.1. Quantum mechanical studies

#### 3.1.1. Geometrical parameters

The optimized geometries of dipeptide, tripeptide, tetrapeptide and hexapeptide structures at MP2/6-31G (d,p) level of theory are shown in Fig. 3 for gas and solvent media. Similarly the optimized geometries of all the above peptide structures at B3LYP/6-31G (d,p) and M052X/6-31G (d,p) level of theories are shown in supporting information Fig. S1. The values of bond lengths and bond energies are tabulated in Table 1. The bond length of intramolecular disulfide bond reported at B3LYP/6-31G (d,p) and M052X/6-31G (d,p) level of theories are found to be larger than those calculated by

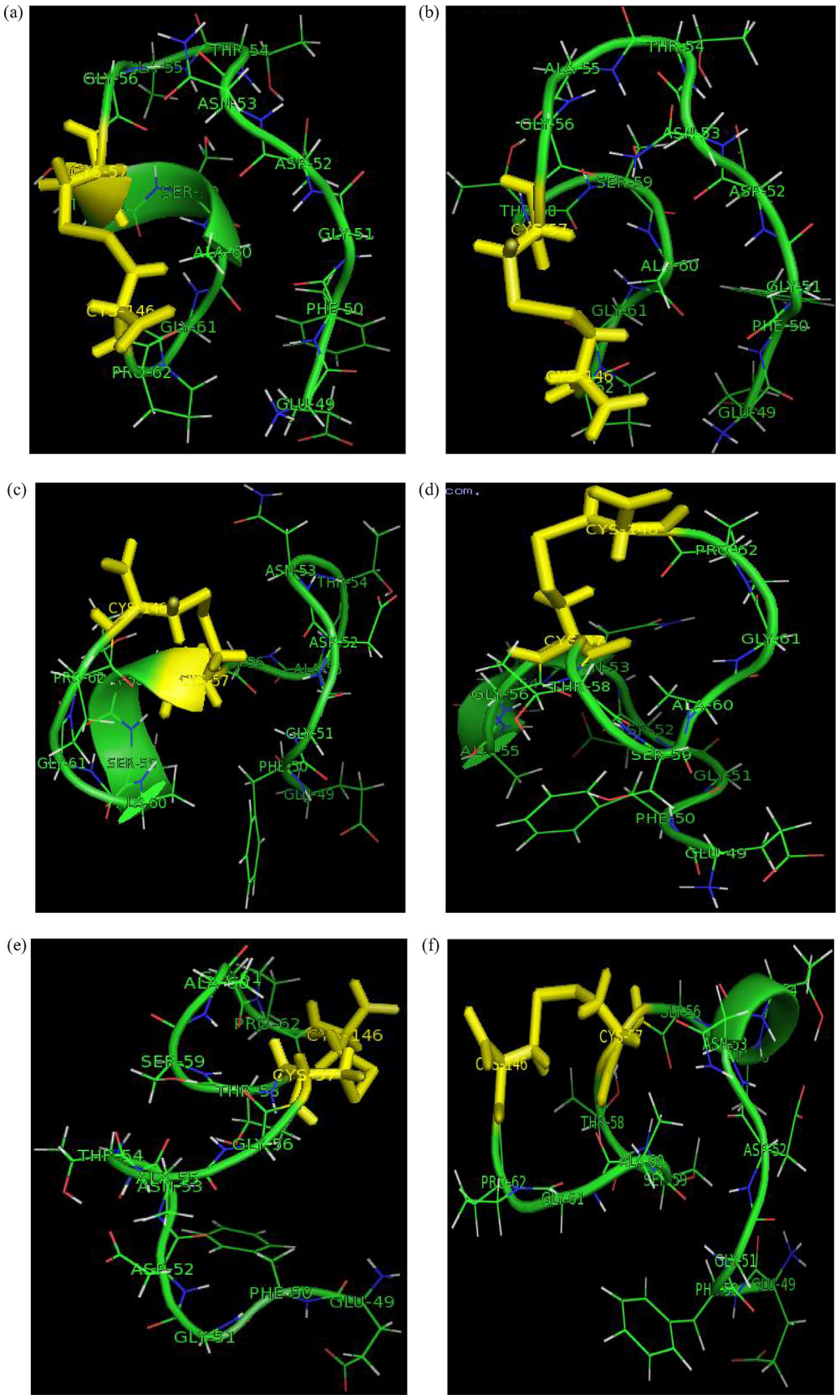


**Fig. 2.** Represents the conformational changes of disulfide loop in 1HL5 and A4V in water environment (a) 1HL5 at 0 ns (b) A4V at 0 ns (c) 1HL5 at 3 ns (d) A4V at 3 ns (e) 1HL5 at 30 ns (f) A4V at 30 ns.

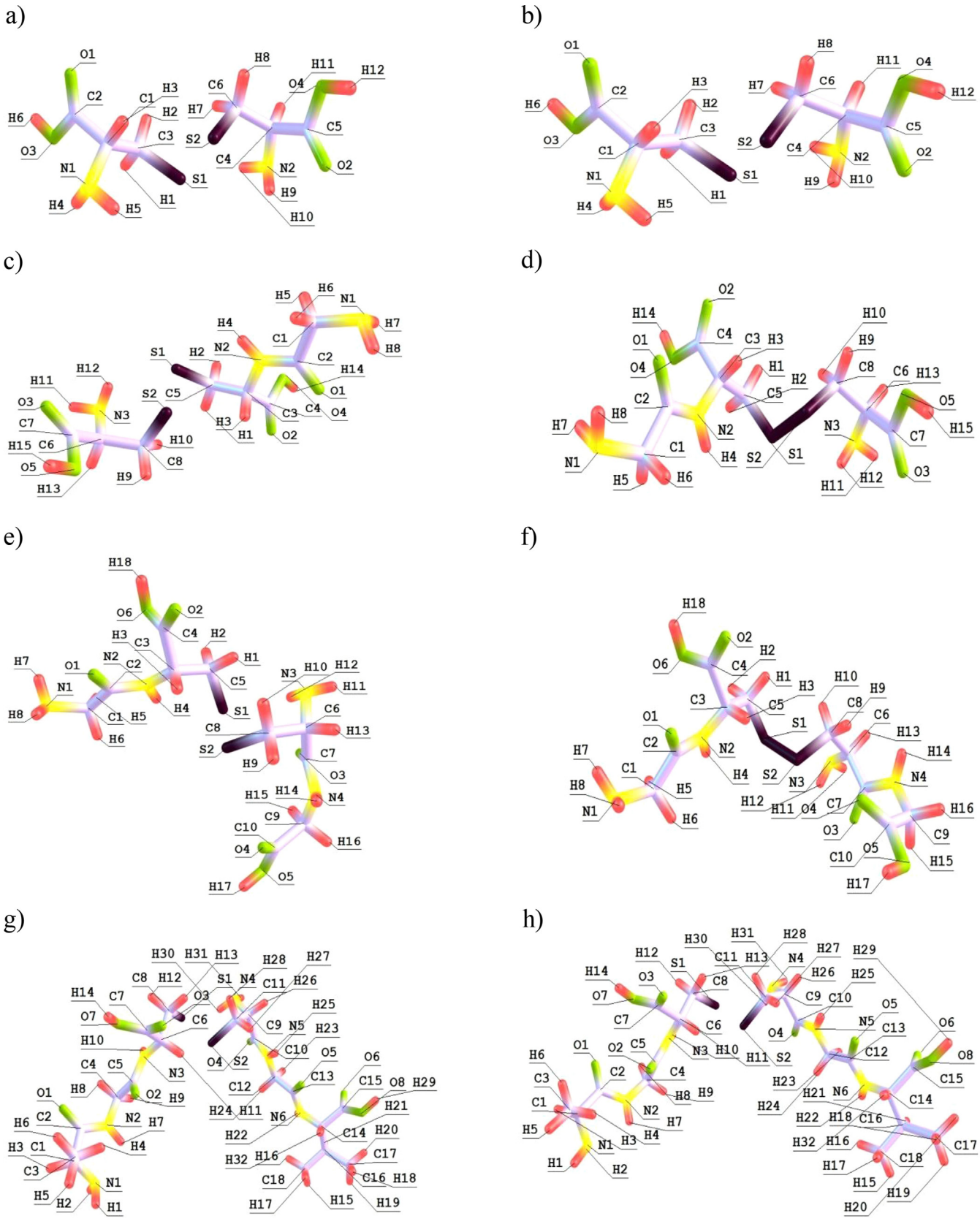


**Fig. 3.** Represents optimized geometry of peptides in MP2/6-31G(d,p) level of theory (a) dipeptide in gas medium (b) dipeptide in solvent medium (c) tripeptide in gas medium (d) tripeptide in solvent medium (e) tetrapeptide in gas medium (f) tetrapeptide in solvent medium (g) hexapeptide in gas medium (h) hexapeptide in solvent medium.

**Table 1**
Bond length compared with experimental data – (a) Gas Phase; (b) solvent phase.

| S.No. | Name of the structure with labelled sulfur atoms | Bond length in different levels of theory in angstorm | | |
|---|---|---|---|---|
| | | B3LYP/6-31G** | M052X/6-31G** | MP2/6-31G** |
| *(a) Bond length compared with experimental data – gas phase* | | | | |
| 1 | S6–S12 (CYS57–CYS146) | 2.089 Å | 2.069 Å | 2.061 Å |
| 2 | S10–S16 (GLY56CYS57–CYS146) | 2.087 Å | 2.067 Å | 2.060 Å |
| 3 | S10–S16 (GLY56CYS57–CYS146GLY147) | 2.085 Å | 2.066 Å | 2.064 Å |
| 4 | S15–S21 (ALA55GLY56CYS57–CYS146GLY147VAL148) | 2.065 Å | 2.065 Å | 2.066 Å |
| *(b) Bond length compared with experimental data – solvent phase* | | | | |
| 1 | S6–S12 (CYS57–CYS146) | 2.090 Å | 2.070 Å | 2.061 Å |
| 2 | S10–S16 (GLY56CYS57–CYS146) | 2.086 Å | 2.067 Å | 2.059 Å |
| 3 | S10–S16 (GLY56CYS57–CYS146GLY147) | 2.083 Å | 2.064 Å | 2.058 Å |
| 4 | S15–S21 (ALA55GLY56CYS57–CYS146GLY147VAL148) | 2.089 Å | 2.066 Å | 2.066 Å |

**Table 2**
Bond energy for different structures in (a) gas phase and (b) solvent phase in different levels of theories.

| S.No. | Name of the structure with labelled sulfur atoms | Bond energy in different levels of theory in kcal/mol | | |
|---|---|---|---|---|
| | | B3LYP/6-31G** | M052X/6-31G** | MP2/6-31G** |
| *(a) Bond energy for different structures in gas phase in different levels of theories* | | | | |
| 1 | S6–S12 (CYS57–CYS146) | 54.47 | 59.46 | 59.53 |
| 2 | S10–S16 (GLY56CYS57–CYS146) | 57.91 | 58.37 | 59.68 |
| 3 | S10–S16 (GLY56CYS57–CYS146GLY147) | 57.09 | 58.49 | 59.84 |
| 4 | S15–S21 (ALA55GLY56CYS57–CYS146GLY147VAL148) | 58.98 | 59.00 | 60.01 |
| *(b) Bond energy for different structures in solvent phase in different levels of theories* | | | | |
| 1 | S6–S12 (CYS57–CYS146) | 55.88 | 58.53 | 59.43 |
| 2 | S10–S16 (GLY56CYS57–CYS146) | 56.15 | 58.65 | 59.65 |
| 3 | S10–S16 (GLY56CYS57–CYS146GLY147) | 56.35 | 58.55 | 59.79 |
| 4 | S15–S21 (ALA55GLY56CYS57–CYS146GLY147VAL148) | 56.69 | 58.82 | 59.88 |

MP2/6-31G (d,p) level of theory. The bond lengths and bond energies of disulfide bond in various peptide structures at MP2/6-31G (d,p) level of theory in gas and solvent phases are close to the experimental value of 2.059 Å [36]. The intramolecular disulfide bond in native SOD1 protein between two cysteine residues 57 and 146, is found to be 2.06 Å at MP2/6-31G (d,p) level of theory, the same bond length is found to be 2.09 and 2.07 Å at B3LYP/6-31G (d,p) and M052X/6-31G (d,p) level of theories respectively. A similar trend has been found for bond length values observed for structures with additional residues added to the terminal of each cysteine residues forming intramolecular disulfide bond. The disulfide bond being a covalent bond requires 60 kcal/mol of energy to pull the two sulfur atoms apart. The bond energies of disulfide bond in various peptides have been listed in Table 2. The shorter bond lengths were found to possess more bond energy leading to the increased stability of the S—S covalent bond. The covalent interaction between the two sulfur atoms of Cys 57 and Cys 146 is confirmed by the bond energy. This is supported by the fact that for smaller distance between two atoms, the system requires a larger rupture force [37]. Thus the disulfide bond strength is found to be sufficient to maintain the stability, folding and proper functioning of the protein.

### 3.1.2. Binding energy

The binding energy between the two sulfur atoms of cysteine residues 57 and 146 is tabulated in Table 3. The binding affinity between the S—S atoms is found to be unaffected while adding the additional residues. The binding energies have been corrected for the basis set superposition error [BSSE] using the counterpoise correction method of Boys and Bernadi [38],

$$\Delta E = E_{AB} - (E_A + E_B)$$

Where $E_{AB}$ is the energy of the complex system with both the cysteine residues and additional residues, $E_A$ and $E_B$ are the energies of individual cysteines with residues at their terminal. When the number of residues in the complex is increased the secondary interactions are found to be negligibly small so that the binding energy is found to be almost constant for the disulfide bond. The binding energies for different peptide structures are found to be around −24 kcal/mol at MP2/6-31G (d,p) level of theory. In DFT level of theories the binding energies were found to be around −53 and −60 kcal/mol. The significant difference between DFT and MP2 level of theories can be described in terms of electron correlation errors which in result leads to wrong charge transfer between the sulfur atoms of cysteine residues [39]. It is found that the interaction energy is increasing when the distance between the S—S atoms are decreased. The higher stability of the disulfide bond is found to be useful in connecting the metal coordinating loop IV to the central β-sandwich. The stronger disulfide bond supports the dimerization process by maintaining the dimer–interface interactions.

**Table 3**
Binding energy for different structures in gas phase in different levels of theories.

| S.No. | Name of the structure with labelled sulfur atoms | Binding energy in different levels of theory in kcal/mol | | |
|---|---|---|---|---|
| | | B3LYP/6-31G** | M052X/6-31G** | MP2/6-31G** |
| 1. | S6–S12 (CYS57–CYS146) | −53.087 | −60.115 | −24.472 |
| 2 | S10–S16 (GLY56CYS57–CYS146) | −53.401 | −59.864 | −24.410 |
| 3. | S10–S16 (GLY56CYS57–CYS146GLY147) | −53.5892 | −60.240 | −24.159 |
| 4. | S15–S21 (ALA55GLY56CYS57–CYS146GLY147VAL148) | −56.099 | −59.676 | −24.347 |

**Table 4**
Condensed Fukui functions for sulfur atoms indifferent levels of theory – gas phase.

| S.No. | Name of the atom | B3LYP/6-31G** | | | M052X/6-31G** | | | MP2/6-31G** | | |
|---|---|---|---|---|---|---|---|---|---|---|
| | | $f_k^-$ | $f_k^+$ | $f_k^0$ | $f_k^-$ | $f_k^+$ | $f_k^0$ | $f_k^-$ | $f_k^+$ | $f_k^0$ |
| 1 | S6 (dipeptide) | 0.2603 | 0.1246 | 0.192 | 0.3273 | 0.1939 | 0.2603 | 0.3492 | 0.3226 | 0.3360 |
| 2 | S12 (dipeptide) | 0.2266 | 0.1360 | 0.181 | 0.3149 | 0.1739 | 0.2447 | 0.3466 | 0.3090 | 0.3279 |
| 3 | S10 (tripeptide) | 0.3258 | 0.0661 | 0.1960 | 0.3338 | 0.2399 | 0.2864 | 0.2290 | 0.3314 | 0.2802 |
| 4 | S16 (tripeptide) | 0.2973 | 0.1141 | 0.2057 | 0.32085 | 0.2533 | 0.2872 | 0.0680 | 0.3154 | 0.1917 |
| 5 | S10 (tetrapeptide) | 0.2476 | 0.0458 | 0.1467 | 0.3356 | 0.2250 | 0.2808 | 0.2300 | 0.3284 | 0.2792 |
| 6 | S16 (tetrapeptide) | 0.2311 | 0.0946 | 0.1629 | 0.3245 | 0.2666 | 0.2950 | 0.07664 | 0.3211 | 0.1989 |
| 7 | S15 (hexapeptide) | 0.1976 | 0.0533 | 0.1535 | 0.3300 | 0.0902 | 0.2101 | 0.3491 | 0.3248 | 0.3370 |
| 8 | S21 (hexapeptide) | 0.1640 | 0.0274 | 0.0957 | 0.3192 | 0.1441 | 0.2313 | 0.3384 | 0.3142 | 0.3263 |

### 3.1.3. Topological and natural bond analyses

A quantitative description of bonding, non-bonding interactions, electronic structure and reactivity were obtained by the topological analysis of electron density [$\rho(r)$] based on Bader's AIM theory. The local properties $\rho(r)$, $\nabla^2\rho(r)$, and $\varepsilon$ computed at BCP at MP2/6-31G (d,p) level of theory for the conformers obtained by Molecular Dynamics simulation both in solvent and vacuum media are summarized in Tables S1 and S2 in supporting information. The existence of a chemical bond between the atom pair is conditioned by the appearance of bond critical point [BCP] [40]. The $\rho(r)$ value is related to the bond order and can be considered as a measure of bond strength [41]. The conformers which possess electron density $\rho(r) > 0.15$ were found to have pure covalent interactions. The conformer with electron density $\rho(r) < 0.15$ is related to intermediate interactions. The Laplacian of electron density for the conformers of dipeptide, tripeptide, tetrapeptide and hexapeptide structures were found to be less than zero, i.e., $\nabla^2\rho(r) < 0$, which therefore confirms the existence of pure covalent interactions both in solvent and vacuum media. The increment of $\nabla^2\rho(r)$ values from dipeptide to hexapeptide with a negative sign corresponds to large accumulation of charge between the nuclei when additional residues are being added to terminals of cysteine residues. Hence these results confirm the existence of shared interactions between the sulfur atoms. In vacuum medium, the conformers of different peptide structures characterize the disulfide bond by the value of $\rho(r) > 0.15$. The ellipticity is defined as $\varepsilon = |\lambda 1|/\lambda 2 - 1$ as a measure of the relative accumulation of charge in the two directions e1 and e2 perpendicular to bond-path at a BCP [42]. The small ellipticity values at the BCP for the conformers of various peptides indicate the presence of sigma bond between the two sulfur atoms in solvent medium. In vacuum medium, for tripeptide and tetrapeptide, the bond ellipticity is found to vary from other structures both in solvent and vacuum media. Hence they possess the tendency to change from sigma bond to slightly pi bond, because the glycine residues at the terminal of the cysteine residue pulls the cysteine apart and therefore tends to reduce the stability of the bond. But the energy transfer between the sulfur atoms is found to be large so that the disulfide bond is said to remain with its own characteristic feature in case of tripeptide and tetrapeptide.

The natural bond analysis [NBO] has been carried out to study the charge transfer mechanism between the sulfur atoms to maintain the stability of disulfide bond when residues are being added at the terminals of cysteine residues. The transfer of charge from the lone pair donor orbitals to the anti-bonding acceptor orbitals is listed in Tables S3 and S4 in supporting information for both gas and solvent media. The different peptide structures were subjected to NBO analysis in three different levels viz., B3LYP, M052X and MP2 using 6-31G (d,p) basis set both in solvent and gas media. In the case of dipeptide the transfer of charge from S6 to C11–S12 is found to be larger than the S12–C5–S6. Hence the sulfur atom of cysteine 57 is found to contribute more towards the stability of disulfide bond. The stabilization energies of C11–S12···S6 in MP2/6-31G (d,p) level of theory for both gas and solvent medium are 6.70 and 6.81 kcal/mol respectively. For tripeptide both in gas and solvent media the contribution by the sulfur atom of cysteine 146 is found to be more effective to maintain the stability of disulfide bond than the sulfur atom of cysteine 57 where glycine 56 is being attached with it. The stabilization energies of C9–S10···S16 in MP2/6-31G (d,p) level of theory for both gas and solvent medium are 7.42 and 7.22 kcal/mol respectively. In the case of tetrapeptide for gas and solvent media the disulfide bond stability is contributed by the sulfur atom of cysteine 146, because, the transfer of charge from sulfur atom of cysteine 57 to its neighbouring, anti-bonding acceptor orbital is found to be higher. The stabilization energies of C9–S10···S16 in MP2/6-31G (d,p) level of theory for both gas and solvent medium are 6.63 and 7.21 kcal/mol respectively. In hexapeptide the sulfur atom in cysteine 146 contributes more for the stability of disulfide bond than the lone pair donor atom of cysteine 57, because the charge transferred to the nearest C11–C14 and C14–H45 anti-bonding acceptor orbitals is found to be higher than the charge transferred from the sulfur atom of cysteine 146 to its nearest C17–C20 andC20–H61 anti-bonding acceptor orbitals. The stabilization energies of C14–S15···S21 in MP2/6-31G (d,p) level of theory for both gas and solvent medium are 7.33 and 7.13 kcal/mol respectively. This result is found to be consistent for both, gas and solvent media.

### 3.1.4. Reactive indices calculation and Potential Energy Scan [PES]

Table 4 depicts the values of $f_k^+(r)$, $f_k^-(r)$ and $f_k^0(r)$ of sulfur atoms in Cys 57 and Cys 146 residues. The values were calculated by MPA at B3LYP/6-31G (d,p), M052X/6-31G (d,p) and MP2/6-31G

**Table 5**
Phillicity for sulfur atoms indifferent levels of theory – gas phase.

| S.No. | Name of the atom | B3LYP/6-31G** | | | M052X/6-31G** | | | MP2/6-31G** | | |
|---|---|---|---|---|---|---|---|---|---|---|
| | | $w_k^-$ | $w_k^+$ | $w_k^0$ | $w_k^-$ | $w_k^+$ | $w_k^0$ | $w_k^-$ | $w_k^+$ | $w_k^0$ |
| 1 | S6 (dipeptide) | 0.0246 | 0.0118 | 0.0182 | 0.0220 | 0.0130 | 0.0175 | 0.0123 | 0.0114 | 0.0119 |
| 2 | S12 (dipeptide) | 0.0214 | 0.0128 | 0.00171 | 0.0211 | 0.0116 | 0.01642 | 0.0122 | 0.0109 | 0.0116 |
| 3 | S10 (tripeptide) | 0.0338 | 0.0068 | 0.0203 | 0.0253 | 0.0181 | 0.0217 | 0.0081 | 0.0118 | 0.0099 |
| 4 | S16 (tripeptide) | 0.0309 | 0.01187 | 0.0214 | 0.0243 | 0.0192 | 0.0217 | 0.0024 | 0.0112 | 0.0068 |
| 5 | S10 (tetrapeptide) | 0.0244 | 0.00453 | 0.0145 | 0.0242 | 0.01623 | 0.0202 | 0.0065 | 0.0093 | 0.0079 |
| 6 | S16 (tetrapeptide) | 0.0228 | 0.0093 | 0.0160 | 0.0234 | 0.0192 | 0.0213 | 0.0021 | 0.0091 | 0.0056 |
| 7 | S15 (hexapeptide) | 0.0158 | 0.0042 | 0.0123 | 0.0230 | 0.0063 | 0.0146 | 0.0416 | 0.0388 | 0.0401 |
| 8 | S21 (hexapeptide) | 0.0131 | 0.0022 | 0.0076 | 0.0223 | 0.01006 | 0.0161 | 0.0403 | 0.0374 | 0.3263 |

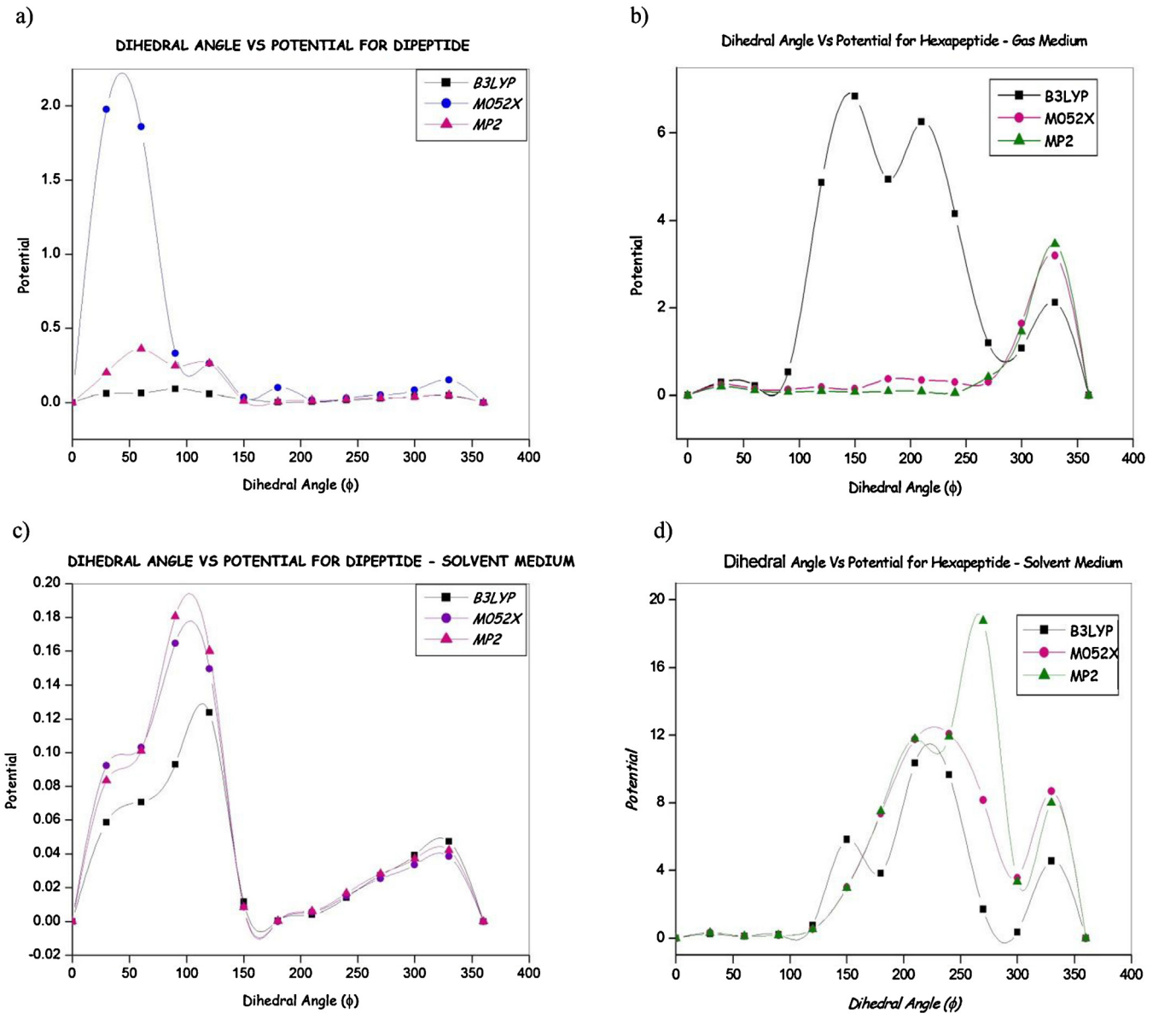


**Fig. 4.** Represents the potential energy against the dihedral angle for (a) dipeptide in gas medium (b) hexapeptide in gas medium (c) dipeptide in solvent medium (d) hexapeptide in solvent medium.

(d,p) level of theories. The sulfur atoms are considered as the most reactive site for electrophilic, nucleophilic and radical attacks. The reactivity of both the sulfur atoms was calculated using the definition of electrophilicity provided by Parr and co-workers [43].

$$\omega = \frac{\mu^2}{2\eta} = \frac{\chi^2}{2\eta}$$

It is also possible to define a local quantity called philicity which is associated with a site $k$ in a molecule with the help of the corresponding condensed to atom variants Fukui function $f_k^\alpha$ as,

$$\omega_k^\alpha = \omega f_k^\alpha$$

$\alpha = +, -$ and 0 representing electrophilic, nucleophilic and radial attacks [44]. The values of philicity index are listed in Table 5. The sulfur atoms S12, S16, S16 and S21 serve as nucleophile (electron donors), the sulfur atoms numbered S6, S10, S10 and S15 are found to act as electrophile (electron acceptors). From the intramolecular disulfide bond formation in SOD1 we found that the sulfur atom of Cys 146 acts as nucleophile while the sulfur atom of Cys 57 acts as electrophile. Hence the protonation is found to occur most preferentially in the sulfur atom of Cys 57. This nature is not disturbed even when number of residues is being added to their termini. We found that the electrophile atoms S6, S10, S10 and S15 are found to possess higher electrophilicity; similarly the nucleophile atoms S12, S16, S16, and S21 are found to have lower electrophilicity. The

**Table 6**
Energy of The Most Stable Conformers In Gas And Solvent Medium For Mp2/6-31g** Level Of Theory.

| S.No. | Different peptide structures | Conformer energy in Hartree | |
|---|---|---|---|
| | | Gas medium | Solvent medium |
| 1 | Dipeptide | −1439.545 | −1439.6347 |
| 2 | Tripeptide | −1642.110 | −1645.619 |
| 3 | Tetrapeptide | −1854.360 | −1853.997 |
| 4 | Hexapeptide | −2425.800 | −2386.826 |

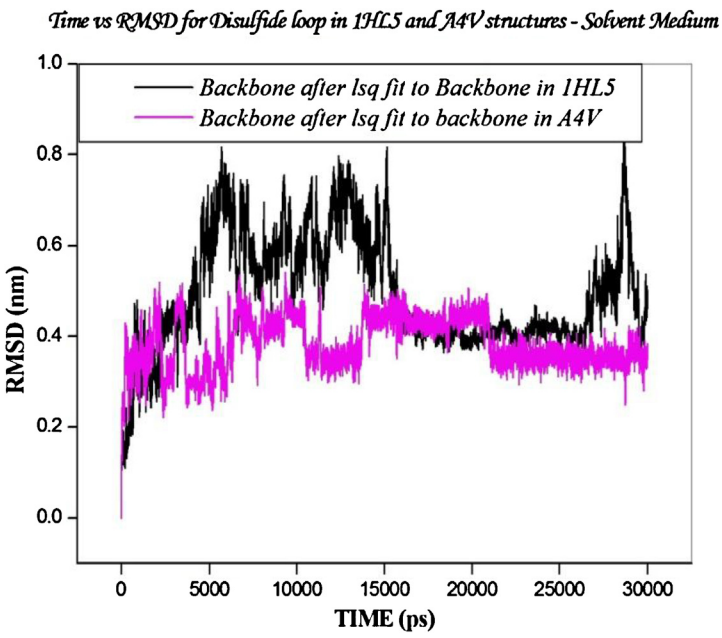


**Fig. 5.** RMSD for backbone atoms of disulfide loop in solvent medium.

reactivity between sulfur atoms is found to be enhanced in the order as follows dipeptide < tetrapeptide ≅ tripeptide < hexapeptide. We concluded that when the number of residues attached with the termini of cysteine residues is increased then the reactivity of the sulfur atoms is also increased.

The energies for the most stable conformers of various peptide structures at MP2/6-31G (d,p) level of theory were listed in Table 6 for gas and solvent media. We obtained different conformers by varying the dihedral angle C3–S1–S2–C4, at each step the geometry was optimized in both the media. To derive the potential function for the internal rotation, the truncated Fourier expansion [45,46] was considered for the potential function $V(\Phi)$ as

$$V(\Phi) = \sum_{i=1}^{6} \frac{1}{2} V_i(1 - \cos(i\Phi))$$

Where $V(\Phi)$ is the relative energy at the rotational angle $\Phi$. When the calculated potentials are plotted against the dihedral angle, we obtained Fourier fitted potential energy curves which are shown in Fig. 4 for the dipeptide and hexapeptide structures for three different level of theories in gas and solvent media, While the potential energy curve for the tripeptide and tetrapeptide in the above level of theories are given in the supporting information Fig. S2 for both the media. The potential energy graph illustrates that the potential energy corresponds to maximum peak was found to be the most stable conformer for the intramolecular disulfide bond in different peptide structures. The maximum peak in the potential–dihedral angle curve, also indicates the highest barrier height for the most stable conformer of disulfide bond in various peptide structures.

### 3.2. Molecular Dynamics analysis

#### 3.2.1. Root mean square deviation [RMSD]

For the native and mutated structures, the disulfide loop of SOD1 monomers in solvent medium is shown in Fig. 5 and for vacuum medium it is shown in the supporting information Fig. S3, indicating the largest displacements between the two structures occurring for the backbone atoms of residues 49–62 and 146. It is shown that the monomers in the native state possess larger RMSD for both the media, because monomers have exposed to a larger hydrophobic patch on the surface of SOD1 to the solvent [47]. In the solvent medium, the RMSD value for disulfide loop is found to be within 0.9 nm, at the native state of SOD1. But for the A4V mutation, the RMSD values are found to be very low around 0.5 nm. The disulfide loop with lower RMSD values in A4V mutation is found to be in good agreement with the local unfolding nature of mutated structures [48]. The minor peaks observed in the disulfide loop of A4V mutant correspond to partial unfolding transition at the temperature of 300 K. In vacuum medium, the RMSD values for disulfide loop in native and mutated SOD1 protein is not fluctuating but remains constant between 0.18–0.22 nm and 0.14–0.18 nm respectively. In the native state of SOD1, the disulfide bond stabilizes the subloop between phenylalanine 50 and alanine 60 and the RMSD values of other residues are almost identical whether or not the disulfide bond is present [49]. In mutated A4V structure, the structural conformations of disulfide loop is found to be varied from the native disulfide loop of SOD1. Hence the disulfide loop is failed to stabilize the subloop leading to misfolding in the mutated state. The regions where the difference between the RMSD values is too large in the two mean minimized structures indicate the conformational differences. During the simulation from 15 to 18 ns, the RMSD values for the two structures are found to be superimposed locally. Therefore the local conformation in this region is well maintained because the structural differences in these regions are found to originate from the translational displacement of the entire region.

#### 3.2.2. Root mean square fluctuation [RMSF]

The RMSF values for the backbone atoms of disulfide loop and entire disulfide loop in native and mutated states of SOD1 protein for a period of 30 ns in solvent medium is shown in Fig. 6 and for vacuum medium, it is given in the supporting information Fig. S4. The distance between the atoms of disulfide loop in A4V mutant differs from the native protein, allowing the peptide segments of the disulfide loop to form the fibrillar aggregates. The higher RMSF value of the native disulfide loop denotes higher conformational flexibility of the residues in the locally unfolded state [48]. The RMSF value of each atom in solvent medium indicate that the disulfide loop

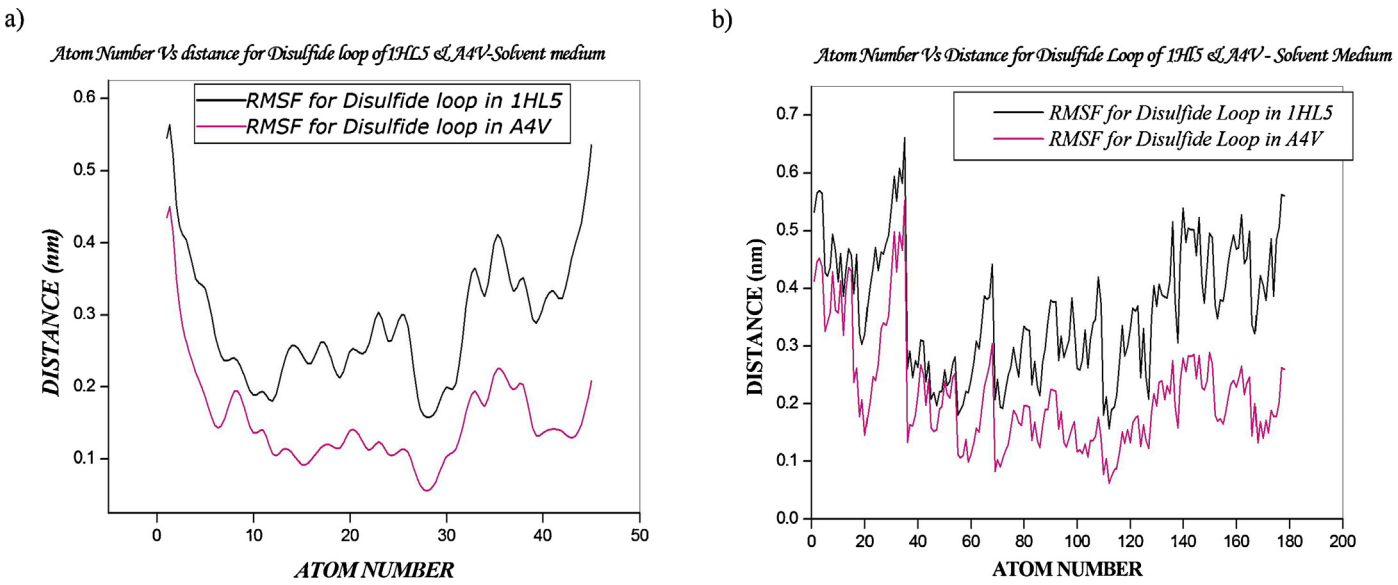


**Fig. 6.** Represents root mean square fluctuations for (a) backbone atoms of disulfide loop in solvent medium and (b) entire disulfide loop in solvent medium.

of A4V mutant are found to be highly disordered, leading to local unfolding of SOD1 than global unfolding. The lower RMSF values also indicate weaker thermo stability of the disulfide loop for A4V mutated protein. In vacuum medium, the RMSF values of disulfide loop were found to be consistent for both native and mutated protein. The RMSF values in solvent medium determine the flexibility of the loop. The fluctuations up to 0.65 nm enable to have larger flexibility of the loop in native SOD1. In solvent medium, the RMSD values are found to be increased rapidly for both the native and mutated structures during the first 0.1 ns. This is because, the crystal structures are found to be relaxed upon solvation in solution [50]. The lower values of RMSD and RMSF for disulfide loop of A4V mutant illustrates that the orientation of disulfide loop differs from the orientation of disulfide loop in native state. In solvent medium the RMSD values of the disulfide loop are found to be increases gradually till 15 ns at constant temperature of 300 K. Hence the increased thermal motion leads to the enhancement of conformational search. The decrease in RMSD values of disulfide loop during the simulation from 15 to 25 ns allows the segment to possess increased number of hydrogen bonds.

### 3.2.3. Radius of gyration [Rg]

The variation of radius of gyration of disulfide loop in native and mutated protein in solvent medium is depicted in Fig. 7 and for vacuum medium it is shown in the supporting information Fig. S5. The backbone atoms are involved in the calculation of radius of gyration. The radius of gyration is found to be reduced for the disulfide loop in A4V mutant, while the wild type SOD1 possess Rg ranging from 0.55 to 1.01 nm. The radius of gyration is found to be within 0.75 nm for A4V mutation. In the native state, it is found that the regular orientation and reorientation of disulfide loop leads to proper folding of the loop during the period of

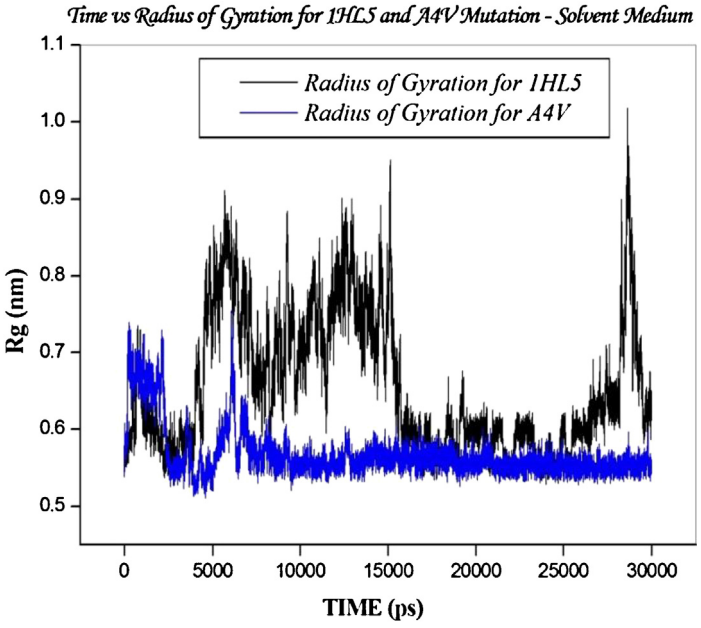


**Fig. 7.** Represents the radius of gyration for disulfide loop in solvent medium.

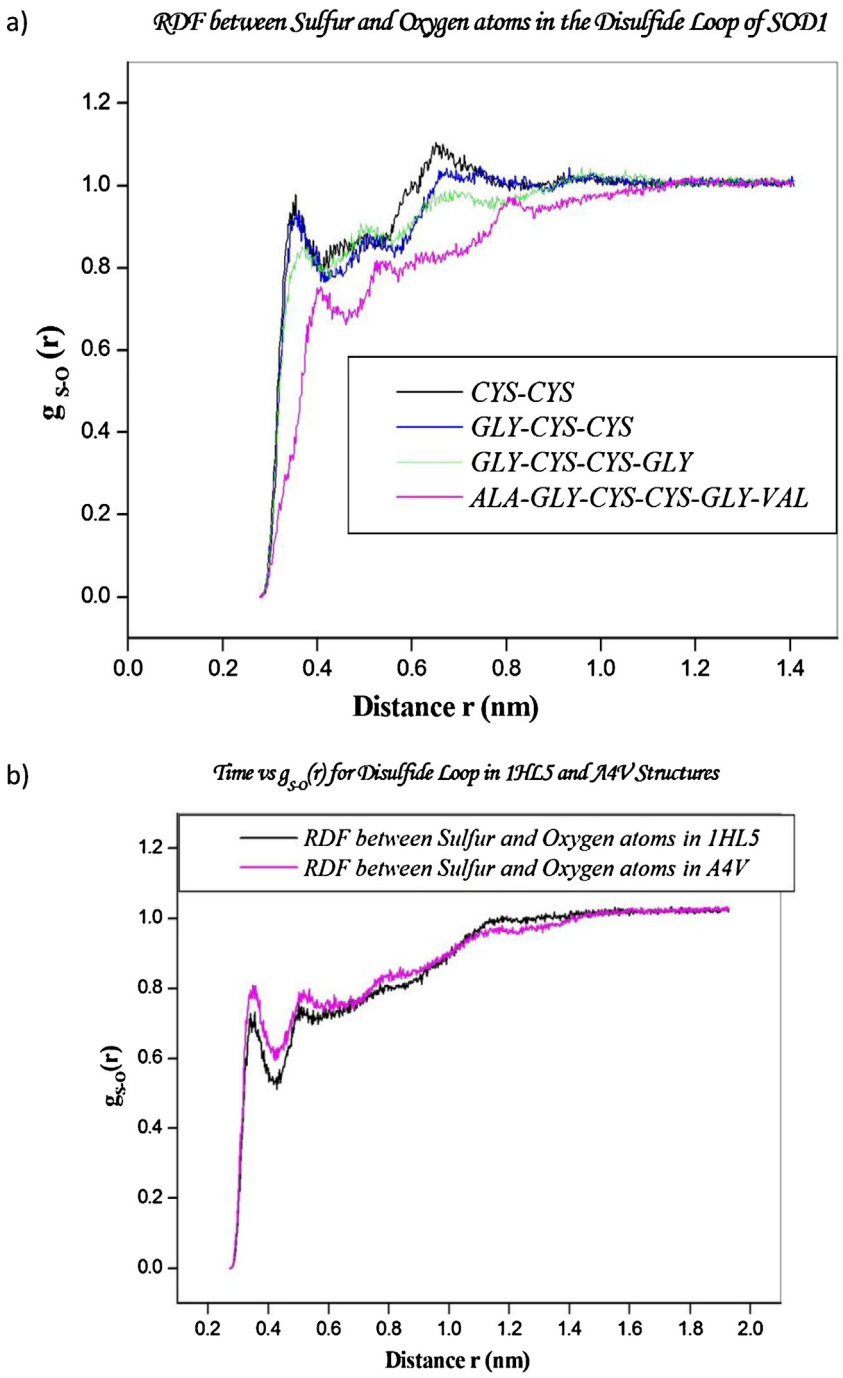


**Fig. 8.** Represents MD results for sulfur–oxygen radial distribution function (a) different kind of peptides (b) for 1HL5 and A4V.

simulation. The small Rg values of A4V mutant indicate the formation of fibrillar aggregates, because the introduction of small population of monomers in the sample would result in smaller Rg values [51]. In vacuum medium, Rg value is found to be constant without any fluctuations during the entire period of simulation. The A4V mutant also has Rg values of disulfide loop lower than the native state in vacuum medium. When the radius of gyration is reduced, the mobility of the atoms is increased. As a result of this, the residues in the disulfide loop of A4V mutant can easily interact with the neighbouring residues and aggregates together. The number of intramolecular hydrogen bond is found to be decreased when the radius of gyration is increased [52]. Both in solvent and vacuum media, the radius of gyration of the disulfide loop in A4V mutant are found to be reduced, thereby leading to increase in the number of non-native intramolecular hydrogen bonds. These non-native hydrogen bonds account for the variation in the conformational flexibility of the molecule. The radius of gyration demonstrates the role of hydrophobic core in the conformational evolution. In the solvent medium, the mutated structure has found to have higher value of Rg around 6 ns. This is because, the protein is found to expand, thereby it creates a void and hence the solvent molecules are able to penetrate into the hydrophobic region present in the disulfide loop. The lower value of Rg for A4V mutant indicates that the disulfide loop is compressed; hence the secondary structure stability is lost accounting for the misfolding of the mutated protein.

*3.2.4. Radial distribution function [RDF]*

The location of first and second minima of the corresponding sulfur—oxygen [S—O] radial distribution function gives the values of the first and second solvation shell radii from dipeptide to hexapeptide are shown in Fig. 8. The peak heights are found to vary with increase in number of residues. The location of first and second minima of S—O on dipeptide, tripeptide, tetrapeptide and hexapeptide are found to be at a distance of 0.4 and 0.53 nm, 0.41 and 0.56 nm, 0.42 and 0.55 nm and 0.46 and 0.57 nm respectively. We found some changes in the location of minima's of S—O bond. The Molecular Dynamics analysis for sulfur—oxygen radial distribution function of disulfide loop in native and mutated states is shown in Fig. 8. The position of first and second solvation shell for S—O of disulfide loop in native state at the distance of 0.42 and 0.56 nm found to be in consistent with first and second coordination shell of disulfide loop in A4V mutant. The maximum peak value in the first coordination shell of native and mutated states was found to be at 0.35 nm. The shallowness of the first minimum in the A4V mutation is found to be decreases in relation with the shallowness of first minimum in native loop. The sharpness of the first coordination shell in the disulfide loop of A4V mutated state is found to be decreases but possess higher amplitude than first coordination shell of disulfide loop in native state. As a result the interactions between sulfur—oxygen are found to be decreased in disulfide loop of A4V mutation. The peaks are found to be flattened nearly after second coordination shell.

The correlation between oxygen atom of C=O group of Cys 57–Cys 146 dipeptide, tripeptide, tetrapeptide and hexapeptide with the hydrogen atoms of water molecules are shown in supporting information Fig. S6. The maximum peak in the first coordination shell of RDF indicates that the hydrogen atoms of nearest water molecules form hydrogen bond with the corresponding oxygen atoms in the C=O group of dipeptide. The inter hydrogen bond distance in the first and second solvation shell of Cys 57–Cys 146 is found to be 0.18 nm and 0.32 nm. Usually in proteins, the hydrogen bond length is found to be ranging from 0.25 to 0.32 nm corresponding to electrostatic interactions [53]. Hence the intermolecular hydrogen bonds in second solvation shell of Cys 57–Cys 146 are found to satisfy the hydrogen bond criteria for protein. In the case of Gly 56–Cys 57, the intermolecular hydrogen bonds in the second solvation shell corresponds to weak electrostatic interactions for tripeptide, tetrapeptide and hexapeptide. In the same way for Cys 146–Gly 147, the second solvation shell exhibit weak and moderate electrostatic interactions for tetrapeptide and hexapeptide. In the case of hexapeptide for Ala 55–Gly 56 and Gly 147–Val 148, the first solvation shell hydrogen bonds corresponds to 0.18 nm and second solvation shell intermolecular hydrogen bonds approaches to 0.32 nm.

## 4. Conclusions

The computational analysis on the bond length and bond energy of disulfide bond in gas and solvent media with the addition of number of residues to the cysteine residues exhibits no change, which paves the way for the disulfide loop to remain in its normal conformation. The binding energy was found to be increased with the increase in number of residues. The topological analysis confirms the covalent characteristics of disulfide bond both in gas and solvent media. The interactions between the sulfur atoms of discontinuous residues were characterized by the properties exhibited by the electron density at BCP. From the reactive indices calculation, it was found that sulfur atom of Cys 57 serves as an electrophile while the sulfur atom of Cys 146 serves as a nucleophile, which was also confirmed by the electrophilicity index calculations. The potential energy curve of disulfide loop in various peptide structures using the truncated Fourier series expansion illustrates that the potential at the maximum peak height was found to have higher stability than the other conformers. The charge transfer between the sulfur atoms help to maintain the stability of disulfide bond was confirmed by the NBO analysis. Hence the charge transfer from sulfur atom to its nearest neighbouring anti-bonding molecular orbitals were found to be increased with the increment of residues both in gas and solvent media.

The difference in structural parameters of disulfide loop in mutated structures from native state explains that the coordination of sulfur atoms in disulfide loop is responsible for neurotoxicity in mutant SOD1. The distance between the sulfur atoms is found to be unaffected with the addition of residues to the terminal of cysteine residues by MD simulation. This confirms the fact the disulfide loop with large number of residues remains unaltered due to mutation. In A4V mutation, the RDF values between the sulfur–oxygen atoms are found to have reduced correlation between the atoms than in disulfide loop of native state. Thus the shift or decrease in the atom–atom contact leads to destabilization of the dimer in SOD1 protein because of this A4V was found to have less stability than wild type protein. The variation in the RMSD and RMSF values of the A4V mutant explains how the mutation takes place in a place other than disulfide loop can create crinkled appearance on the disulfide loop ribbons resulting in different folding patterns that eventually affects the metal binding and overall protein stability. Thus the Molecular Dynamics simulation of disulfide loop in native and mutated states elucidates the structural changes by different conformers at various nanoseconds. Thus the non-native conformations of the disulfide loop and reduced radius of gyration for A4V mutant explain that the flexibility of the disulfide loop was reduced.

## Acknowledgements

The authors express their sincere thanks to HPCF Centre (High Performance Computing Facility) of DST Government of India at Hyderabad for allowing us to use the facility, where most of the calculations have been performed.

## Appendix A. Supplementary data

Supplementary data associated with this article can be found, in the online version, at http://dx.doi.org/10.1016/j.jmgm.2014.03.002.

## References

[1] Z. You, X. Cao, A.B. Taylor, P.J. Hart, R.L. Levine, Characterization of a covalent polysulfane bridge in copper–zinc superoxide dismutase, Biochemistry 49 (2010) 1191–1198.
[2] L. Banci, I. Bertini, O. Blazevits, V. Calderone, F. Cantini, J. Mao, A. Trapananti, M. Vieru, I. Amori, M. Cozzolino, M.T. Carri, Interaction of cisplatin with human superoxide dismutase, J. Am. Chem. Soc. 134 (2012) 7009–7014.
[3] H.X. Deng, Y. Shi, Y. Furukawa, H. Zhai, R. Fu, E. Liu, G.H. Gorrie, M.S. Khan, W.Y. Hung, E.H. Bigio, T. Lukas, M.C. Dal Canto, T.V. O'Halloran, T. Siddique, Conversion to the amyotrophic lateral sclerosis phenotype is associated with intermolecular linked insoluble aggregates of SOD1 in mitochondria, Proceedings of National Academy of Sciences, USA 103 (2006) 7142–7147.
[4] M. Chattopadhyay, A. Durazo, S.H. Sohn, C.D. Strong, E.B. Gralla, J.P. Whitelegge, J.S. Valentine, Initiation and elongation in fibrillation of ALS-linked superoxide dismutase, Proceedings of National Academy of Sciences, USA 105 (2008) 18663–18668.
[5] N. Fujiwara, M. Nakano, S. Kato, D. Yoshihara, T. Ookawara, H. Eguchi, N. Taniguchi, K. Suzuki, Oxidative modification to cysteine sulfonic acid of Cys111 in human copper–zinc superoxide dismutase, J. Biol. Chem. 282 (2007) 35933–35944.
[6] Z. You, X. Cao, A.B. Taylor, P.J. Hart, R.L. Levine, Characterization of a covalent polysulfane bridge in Cu,Zn superoxide dismutase, Biochemistry 49 (2010) 1–20.

[7] A. Hörnberg, D.T. Logan, S.L. Marklund, M. Oliveberg, The coupling between disulphide status, metallation and dimer interface strength in Cu/Zn superoxide dismutase, J. Mol. Biol. 365 (2007) 333–342.
[8] J.A. Tainer, E.D. Getzoff, K.M. Beem, J.S. Richardson, D.C. Richardson, Determination and analysis of the 2 Å-structure of copper, zinc superoxide dismutase, J. Mol. Biol. 160 (1982) 181–217.
[9] L.F. Zou, Y. Fu, K. Shen, Q.-X. Guo, Sulfur–sulfur bond dissociation enthalpies: a high-level ab initio study, J. Mol. Struct. 807 (2007) 87–92.
[10] D.P. Patel, Amyotrophic Lateral Sclerosis, Spring, 2010.
[11] D.R. Borchelt, M.K. Lee, H.S. Slunt, M. Guarnieri, Z.S. Xu, P.C. Wong, R.H. Brown Jr., D.L. Price, S.S. Sisodia, D.W. Cleveland, Superoxide dismutase 1 with mutations linked to familial amyotrophic lateral sclerosis possesses significant activity, Proceedings of National Academy of Sciences USA 91 (1994) 8292–8296.
[12] J. Niwa, S. Yamada, S. Ishiqaki, J. Sone, M. Takahashi, M. Katsuno, F. Tanaka, M. Doyu, G. Sobue, Disulfide bond mediates aggregation, toxicity, and ubiquitylation of familial amyotrophic lateral sclerosis-linked mutant SOD1, J. Biol. Chem. 282 (2007) 28087–28095.
[13] K.G. Reddie, K.S. Carroll, Expanding the functional diversity of proteins through cysteine oxidation, Curr. Opin. Chem. Biol. 12 (2008) 746–754.
[14] L. Leinartaite, K. Saraboji, A. Nordlund, D.T. Logan, M. Oliveberg, Folding catalysis by transient coordination of $Zn^{2+}$ to the Cu ligands of the ALS-associated enzyme Cu/Zn superoxide dismutase 1, J. Am. Chem. Soc. 132 (2010) 13495–13504.
[15] R.W. Strange, S. Antonyuk, M.A. Hough, P.A. Doucette, J.A. Rodriguez, P.J. Hart, L.J. Hayward, J.S. Valentine, S.S. Hasnain, The structure of holo and metal-deficient wild-type human Cu,Zn superoxide dismutase and its relevance to familial amyotrophic lateral sclerosis, J. Mol. Biol. 328 (2003) 877–891.
[16] F.C. Bernstein, T.F. Koetzle, G.J. Williams, E.E. Meyer Jr., M.D. Brice, J.R. Rodgers, O. Kennard, T. Shimanouchi, M. Tasumi, The protein data bank: a computer-based archival file for macromolecular structures, J. Mol. Biol. 112 (1977) 535–542.
[17] T. Ratovitski, L.B. Corson, J. Strain, P. Wong, D.W. Cleveland, V.C. Culotta, D.R. Borchelt, Variation in the biochemical/biophysical properties of mutant superoxide dismutase 1 enzymes and the rate of disease progression in familial amyotrophic lateral sclerosis kindreds, Hum. Mol. Genet. 8 (1999) 1451–1460.
[18] G.W. Frisch, H.B. Trucks, G.E. Schlegel, M.A. Scuseria, J.R. Robb, G. Cheeseman, V. Scalmani, B. Barone, G.A. Mennucci, H. Petersson, M. Nakatsuji, X. Caricato, H.P. Li, A.F. Hratchian, J. Izmaylov, G. Bloino, J.L. Zheng, M. Sonnenberg, M. Hada, K. Ehara, R. Toyota, J. Fukuda, M. Hasegawa, T. Ishida, Y. Nakajima, O. Honda, H. Kitao, T. Nakai, J.A. Vreven, Montgomery Jr., J.E. Peralta, M.F. ogliaro, J.J. Bearpark, E. Heyd, K.N. Brothers, V.N. Kudin, R. Staroverov, J. Kobayashi, K. Normand, A. Raghavachari, J.C. Rendell, S.S. Burant, J. Iyengar, M. Tomasi, N. cossi, J.M. Rega, M. Millam, J.E. Klene, J.B. Knox, Cross, C.V. Bakken, J. Adamo, R. Jaramillo, R.E. Gomperts, O. Stratman, A.J. Yazyev, R. Austin, C. Cammi, J.W. Pomeli, R.L. Ochterski, K. Martin, V.G. Morokuma, G.A. Zakrzewski, P. Voth, J.J. Salvador, S. Dannenberg, A.D. Dapprich, O. Daniels, J.B. Farkas, J.V. Foresman, J. Ortiz, D.J. Cioslowski, T. Fox, Gaussian 09, Gaussian, Inc., Wallingford, CT, 2009.
[19] A.D. Becke, Density-functional thermochemistry. III. The role of exact exchange, J. Chem. Phys. 98 (1993) 5648–5652.
[20] A.D. Becke, Density-functional exchange-energy approximation with correct asymptotic behaviour, Physical Review A 38 (1998) 3098–3100.
[21] Y. Zhao, D.G. Truhlar, A density functional that accounts for medium-range correlation energies in organic chemistry, Org. Lett. 8 (2006) 5753–5755.
[22] Y. Zhao, N.E. Schultz, D.G. Truhlar, Design of density funtionals by combining the method of constraint satisfaction with parameterization for thermochemistry, thermochemical kinetics, and noncovalent interactions, Journal of Chemical Theory and Computation 2 (2006) 364–382.
[23] C. Moller, M.S. Plesset, Note on an approximation treatment for many-electron systems, Physical review 46 (1934) 618–622.
[24] A.E. Reed, L.A. Curtiss, F. Weinhold, Intermolecular interactions from a natural bond orbital, donor–acceptor viewpoint, Chem. Rev. 88 (1988) 899–926.
[25] R.F.W. Bader, Atoms in Molecules: International Series of Monographs on Chemistry, A Quantum Theory, vol. 22, Oxford University Press, Oxford, 2009.
[26] D. van der Spoel, E. Lindahl, B. Hess, A.R. van Buuren, E. Apol, P.J. Meulenhoff, D.P. Tieleman, A.L.T.M. Sijbers, K.A. Feenstra, R. van Drunen, H.J.C. Berendsen, Gromacs User Manual Version 4.5.4, 2010 www.gromacs.org
[27] G.A. Kaminski, R.A. Friensner, J. Tirado-Rives, W.L. Jorgensen, Evaluation and reparametrization of the OPLS-AA force field for proteins via comparison with accurate quantum chemical calculations on peptides, J. Phys. Chem. B 105 (2001) 6474–6487.
[28] J.W. Ponder, D.A. Case, Force field for protein simulations, Adv. Protein Chem. 66 (2003) 27–85.
[29] H.J.C. Berendsen, J.P.M. Postma, W.F. Van Gunsteren, J. Hermans, Interaction models for water in relation to protein hydration, in: Intermolecular Forces, D. Reidel Publishing Company Pullman (editor), 1981, pp. 331–342.
[30] I.H. Shrivastava, M.S. Sansom, Simulations of ion permeation through a potassium channel: molecular dynamics of KcsA in a phospholipid bilayer, Biophys. J. 78 (2000) 557–570.
[31] P.B. Moore, C.F. Lopez, M.L. Klein, Dynamical properties of hydrated lipid bilayer from a multinanosecond molecular dynamics simulation, Biophys. J. 81 (2001) 2484–2494.
[32] U. Essmann, L. Perera, M.L. Berkowitz, T. Darden, H. Lee, L.G. Pedersen, A smooth particle mesh Ewald method, J. Chem. Phys. 103 (1995) 8577–8594.
[33] T. Darden, D. York, L. Pedersen, Particle Mesh Ewald: an Nlog(N) method for Ewald sums in large systems, J. Chem. Phys. 98 (1993) 10089–10092.
[34] T.E. Cheatham, J.L. Miller, T. Fox, T.A. Darden, P.A. Kollman, Molecular dynamics simulations on solvated biomolecular systems: the particle Mesh Ewald method leads to stable trajectories of DNA, RNA, and proteins, J. Am. Chem. Soc. 117 (1995) 4193–4194.
[35] M. Saeed, Y. Yang, H-X. Deng, W-Y. Hung, N. Siddique, L. Dellefave, C. Gellera, P.M. Amderson, T. Siddique, Age and founder effect of SOD1 A4V mutation causing ALS, Neurology 72 (2009) 1634–1639.
[36] L.S. Higashi, M. Lundeen, K. Seff, Empirical relations between disulfide bond lengths, (N or C)–C–S–S torsion angles, and substituents in aromatic disulfides. Crystal and molecular structure of 3, 3′-dihydroxydi-2-pyridyl disulfide, J. Am. Chem. Soc. 78 (1997) 8101–8106.
[37] C.-c. Chou, M.J. Buehler, Bond energy effects on strength, cooperativity and robustness of molecular structures, Interface Focus 1 (2011) 734–743.
[38] S.F. Boys, F. Bernadi, The calculation of small molecular interactions by the differences of separate total energies. Some procedures with reduced errors, Mol. Phys. 19 (1970) 553–566.
[39] C. Cazorla, S.A. Shevlin, Accuracy of density functional theory in the prediction of carbon dioxide adsorbent materials, Dalton Transactions 42 (2013) 4670–4676.
[40] A. May, N. Ouddai, Topological analysis of bonding in $[Ru_5(\mu_4\text{-}C_2)L(CO)_{13}]$ and $[Ru_4(\mu_4\text{-}C_2)L(CO)_{10}]$ complexes ($L=(\mu_4\text{-SMe})\ (\mu\text{-}PPh_2)_2$), J. Struct. Chem. 53 (2012) 220–227.
[41] V. Nirmala, P. Kolandaivel, Molecular interaction of $H_2$ and $H_2O$ molecules with the boron nitride $(BN)_{n=3-5}$ clusters: a theoretical study, J. Mol. Struct. 758 (2006) 9–15.
[42] S. Mitra, A.K. Chandra, P.M. Gashnga, S. Jenkins, S.R. Kirk, Exploring hydrogen bond in the excited state leading toward intramolecular proton transfer: detailed analysis of the structure and charge density topology along the reaction path using QTAM, Journal of Molecular Modelling 18 (2012) 4225–4237.
[43] P.K. Chattaraj, A. Chakraborty, S. Giri, Net electrophilicity, J. Phys. Chem. A 113 (2009) 10068–10074.
[44] R. Parthasarathi, J. Padmanabhan, M. Elango, V. Subramanian, P.K. Chattaraj, Intermolecular reactivity through the generalized philicity concept, Chem. Phys. Lett. 394 (2004) 225–230.
[45] P.G. Kolandaivel, N. Kuze, T. Sakaizumi, O. Ohashi, K. Iijima, Molecular structures and rotational potential energy surfaces of E and Z geometrical isomers of propionaldehyde oxime: ab initio and DFT studies, J. Phys. Chem. A 101 (1997) 2873–2878.
[46] L. Random, J.A. Pople, Molecular orbital theory of the electronic structure of organic compounds. IV. Internal rotation in hydrocarbons using minimal Slater-type basis, J. Am. Chem. Soc. 92 (1970) 4786–4795.
[47] S.D. Khare, M. Caplow, N.V. Dokholyan, FALS mutations in Cu,Zn superoxide dismutase destabilize the dimer and increase dimer dissociation propensity: a large-scale thermodynamics analysis, Amyloid 14 (2006) 226–235.
[48] F. Ding, Y. Furukawa, N. Nukina, N.V. Dokholyan, Local unfolding of Cu,Zn superoxide dismutase monomer determines the morphology of fibrillar aggregates, J. Mol. Biol. 421 (2012) 548–560.
[49] F. Ding, N.V. Dokholyan, Dynamical roles of metal ions and the disulfide bond in Cu,Zn superoxide dismutase folding and aggregation, Proceedings of National Academy of Sciences, USA 105 (2008) 19696–19701.
[50] M. Mori, B. Jimenez, M. Piccioli, A. Battistoni, M. Sette, Solution structure of the monomeric copper, zinc superoxide dismutase from *Salmonella enterica*: structural insights to understand the evolution toward the dimeric structure, Biochemistry 47 (2008) 12954–12963.
[51] M.A. Hough, J.G. Grossmann, S.V. Antonyuk, R.W. Strange, P.A. Doucette, J.A. Rodriguez, L.J. Whitson, P.J. Hart, L.J. Hayward, J.S. Valentine, S.S. Hasnain, Dimer destabilization in superoxide dismutase may result in disease-causing properties: structures of motor neuron disease mutants, Proceedings of National Academy of Sciences, USA 101 (2004) 5976–5981.
[52] D.B. Kony, P.H. Hunenberger, W.F. van Gunsteren, Molecular dynamics simulations of the native and partially folded states of ubiquitin: influence of methanol cosolvent, pH, and temperature on the protein structure and dynamics, Protein Sci. 16 (2007) 1101–1118.
[53] A.G. Jeffrey, An introduction to Hydrogen Bonding, Oxford University Press, New York, 1997.